Visualization of DNA-induced conformational changes in the DNA repair kinase DNA-PKcs

Jasminka Boskovic, Angel Rivera-Calzada, Joseph D.Maman[1], Pablo Chacón, Keith R.Willison[2], Laurence H.Pearl[1] and Oscar Llorca[3]

Centro de Investigaciones Biológicas, Consejo Superior de Investigaciones Científicas (CSIC), Ramiro de Maeztu, 9, Campus Universidad Complutense, 28040 Madrid, Spain, [1]Section of Structural Biology and Cancer Research UK DNA Repair Enzyme Research Group and [2]Cancer Research UK Centre for Cell and Molecular Biology, Institute of Cancer Research. Cancer Research UK. Chester Beatty Laboratories, 237 Fulham Road, London SW3 6JB, UK

[3]Corresponding author
e-mail: ollorca@cib.csic.es

J.Boskovic, A.Rivera-Calzada and J.D.Maman contributed equally to this work

The catalytic subunit of the DNA-dependent protein kinase (DNA-PKcs) is essential for the repair of double-stranded DNA breaks (DSBs) in non-homologous end joining (NHEJ) and during V(D)J recombination. DNA-PKcs binds single- and double-stranded DNA *in vitro*, and *in vivo* the Ku heterodimer probably helps recruit it to DSBs with high affinity. Once loaded onto DNA, DNA-PKcs acts as a scaffold for other repair factors to generate a multiprotein complex that brings the two DNA ends together. Human DNA-PKcs has been analysed by electron microscopy in the absence and presence of double-stranded DNA, and the three-dimensional reconstruction of DNA-bound DNA-PKcs displays large conformational changes when compared with the unbound protein. DNA-PKcs seems to use a palm-like domain to clip onto the DNA, and this new conformation correlates with the activation of the kinase. We suggest that the observed domain movements might help the binding and maintenance of DNA-PKcs' interaction with DNA at the sites of damage, and that these conformational changes activate the kinase.
Keywords: DNA-PK/DNA repair/electron microscopy/NHEJ

Introduction

DNA is constantly being exposed to insults that compromise its integrity and its information content. Ionizing radiation and some chemotherapeutic drugs generate double-stranded DNA breaks (DSBs) that must be repaired to avoid genomic instability (Jackson, 2002). DSBs also appear as intermediates in normal nuclear functions, such as V(D)J recombination in developing mammalian lymphocytes. The main DSB repair mechanism in mammals, known as non-homologous end joining (NHEJ), requires a multiprotein complex built around the DNA-PK kinase, and the same basic processes are also used for V(D)J recombination. Deficiency in components of this pathway has been linked to tumour development (Pierce and Jasin, 2001).

DNA-PK comprises a 469 kDa catalytic subunit (DNA-PKcs) and a DNA targeting partner consisting of the 70 and 86 kDa heterodimeric protein Ku. DNA-PKcs and Ku associate very weakly in the absence of DNA. *In vivo*, Ku appears to recognize DSBs with high affinity as a pre-formed circular assembly, which then helps load DNA-PKcs onto the DNA (DeFazio *et al*., 2002). It is presumed that the DNA-bound Ku–DNA-PKcs complex facilitates the loading and activation of other NHEJ components, such as the ligase IV–XRCC4 complex (Jackson, 2002). Also, two DNA-PKcs molecules can probably interact to bring the two DNA ends together (DeFazio *et al*., 2002). Purified DNA-PKcs binds to single- and double-stranded DNA (dsDNA) ends. This interaction has been intensively demonstrated and characterized using biochemical techniques (Leuther *et al*., 1999; Hammarsten *et al*., 2000; Merkle *et al*., 2002; Martensson and Hammarsten, 2002), surface plasmon resonance (West *et al*., 1998), atomic force microscopy (Yaneva *et al*., 1997) and electron microscopy (EM) (DeFazio *et al*., 2002). Upon DNA binding, DNA-PKcs is activated as a serine/threonine kinase (Leuther *et al*., 1999; Martensson and Hammarsten, 2002). This kinase activity is essential for the DNA-PKcs-dependent repair response but not for the actual recognition of DSBs. Two medium resolution structures of DNA-PKcs obtained by electron microscopy of either single particles (Chiu *et al*., 1998) or 2D crystals (Leuther *et al*., 1999) have been published.

DNA-PKcs belongs to the family of the phosphatidylinositol-3-OH kinase-related kinases (PIKKs) (Jackson, 2002) that in mammals includes two other DNA repair proteins, the ATM and ATR kinases. They are all high molecular weight polypeptides sharing a conserved C-terminal region with homology to the catalytic domain of the phosphatidylinositol-3-OH kinase (Rouse and Jackson, 2002; Shiloh, 2003). ATM, ATR and DNA-PKcs are all implicated in the cell response to DSBs, although each family member has specialized functions (Jackson, 2002; Shiloh, 2003). In order to obtain further insight into the structural basis for DNA recognition by DNA-PKcs and the PIKK family of kinases, we have studied purified protein and DNA-bound complexes by single-particle EM to obtain 3D reconstructions and compare them with those of ATM (Llorca *et al*., 2003).

Results and discussion

DNA-PKcs purification, DNA binding and kinase activation

The purified human DNA-PKcs from HeLa nuclear extract appears as a single silver-stained band in a 4–20% SDS–
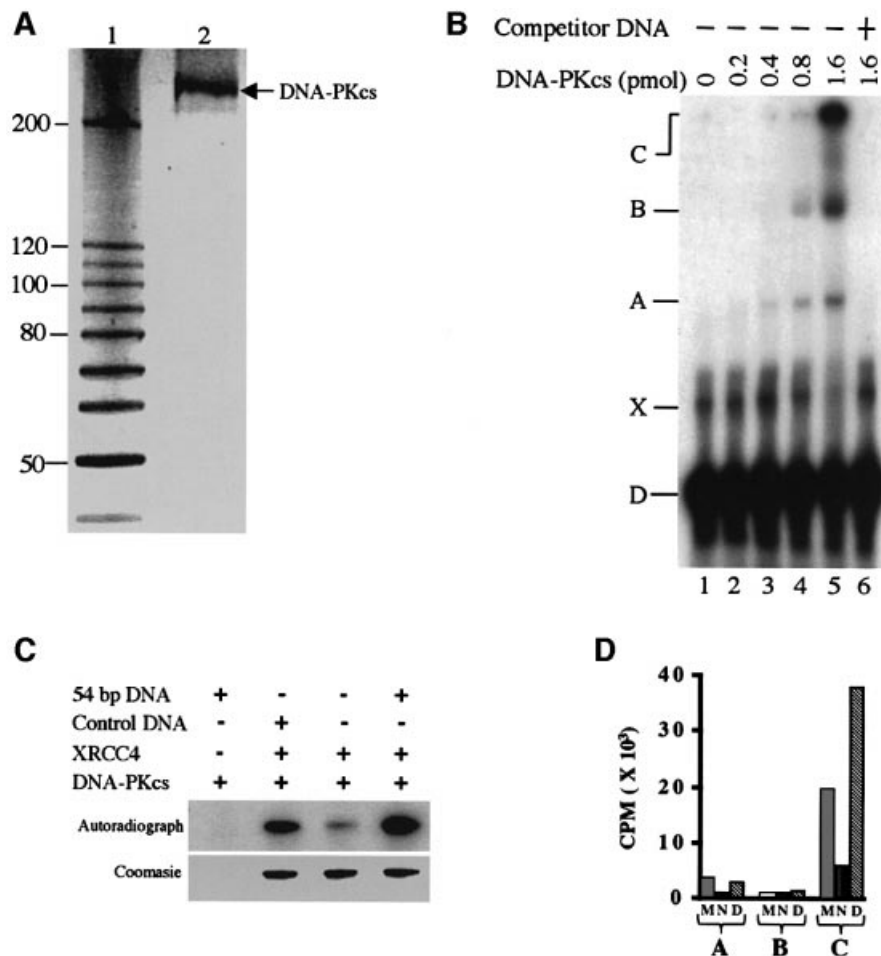
Fig. 1. Purification and functional assays of DNA-PKcs. (**A**) Silver-stained SDS–gel of purified human DNA-PKcs. Lane 1, 10 kDa ladder protein marker (Gibco); lane 2, purified DNA-PKcs. (**B**) EMSA of DNA-PKcs bound to 54 bp DNA. 5′-^{32}P-labelled dsDNA (20 fmol) was titrated with an increasing amount of DNA-PKcs. In lane 6, 500 ng of unlabelled 54 bp DNA were added as competitor. (**C**) Autoradiography of DNA-dependent kinase activity over XRCC4. Protein bands correspond to the XRCC4 in the experiment. Control DNA, 100 bp ladder (New England BioLabs). (**D**) Radioactivity measurement of DNA-dependent kinase activity on DNA-PKcs (autophosphorylation) (lanes A and B) and XRCC4 (lane C). Protein bands obtained in experiments similar to those shown in 'C' were cut and the radioactivity was measured by Cerenkov counting. CPM, counts per minute; A, autophosphorylation of DNA-PKcs in the absence of XRCC; B, autophosphorylation of DNA-PKcs in the presence of XRCC4; C, phosphorylation of XRCC4; M, phosphorylation in the presence of control DNA; N, phosphorylation in the absence of DNA; D, phosphorylation in the presence of 54 bp DNA.

polyacrylamide gel (Figure 1A). Western blot of this protein, probed with an anti-DNA-PKcs antibody (Santa Cruz Biotechnology), also resulted in a single band at the same position (unpublished data). We tested the ability of the purified protein to bind to duplex DNA by electrophoretic mobility shift assay (EMSA) (Figure 1B). We find that DNA-PKcs forms three distinct complexes (lane 5) with 54 bp DNA, and these complexes disappear in the presence of excess unlabelled DNA (lane 6). We did not investigate further the nature of these three complexes, but they have been observed previously (Leuther *et al*., 1999) and it was concluded that complex A contains a single DNA-PKcs molecule, complex B contains two DNA-PKcs molecules and complex C (well position) contains aggregates that arise from protein–protein interactions. Band X, specific to this study, is not a protein–DNA complex because it is present in free DNA (lane 1) and its intensity decreases in the presence of excess DNA-PKcs. We suggest that this band is probably the result of DNA secondary structure as the antisense oligo is capable of forming dimers.

To gain further understanding of the functional relevance of this interaction, we investigated the DNA dependency of DNA-PKcs kinase activity (Figure 1C and D). XRCC4 has been reported to be an excellent substrate for DNA-PKcs, in a DNA-dependent manner (Critchlow *et al*., 1997). The presence of the 54 bp DNA in the kinase reaction increases the phosphorylation of XRCC4 by DNA-PKcs by ~6-fold (Figure 1C, and D lane C), compared with the absence of DNA. Phosphorylation of XRCC4 in the presence of the 54 bp duplex was ~2-fold higher than in the presence of the control DNA (100 bp ladder DNA marker; New England BioLabs), probably because of the higher molar concentration of the 54 bp DNA. As well as phosphorylating several proteins *in vitro*, DNA-PKcs was shown to possess autophosphorylation activity that was DNA dependent (Chan and Lees-Miller, 1996), and we tested this possibility. We show that this autophosphorylation activity is present in our DNA-PKcs preparation (Figure 1D, lanes A and B).
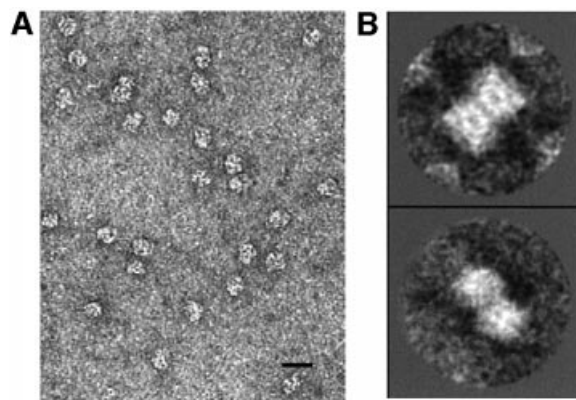
Fig. 2. Electron microscopy. (**A**) EM field from purified DNA-PKcs. Scale bar corresponds to 100 nm. (**B**) 2D averaging of selected dimeric DNA-PKcs.

Electron microscopy of human DNA-PKcs

When the purified protein was adsorbed to carbon-coated grids, negatively stained and observed in the electron microscope, we found a clean distribution of particles in different orientations (Figure 2A). Apparently, and as later confirmed, most of the particles in the EM fields corresponded to DNA-PKcs monomers, but a small percentage of images (<5%) were found to form dimers. Though the number of 'dimer' images collected was not very high, we managed to obtain some 2D averages (Figure 2B) that suggested that they could consist of two molecules joined side by side. The significance of our DNA-PKcs dimers is unclear, but they may reflect an intrinsic ability of the DNA-PKcs monomers to interact with each other. Such a property might be relevant for its regulation through autophosphorylation, since several reports indicate that a DNA-PKcs molecule can phosphorylate another molecule *in trans* (Chan and Lees-Miller, 1996; Soubeyrand *et al.*, 2003). Alternatively, and as proposed for ATM (Bakkenist and Kastan, 2003), the dimers might reflect a regulatory mechanism or an intermediate in the NHEJ repair process (DeFazio *et al.*, 2002).

3D structure of DNA-PKcs

We designed a strategy to analyse the structure of DNA-PKcs and its DNA-bound complexes. As a first control, 2746 single molecule images of DNA-PKcs were extracted from the micrographs and used in a reference-free iterative refinement process (Ludtke *et al.*, 1999; Llorca *et al.*, 2001), resulting in a 3D volume (unpublished data). DNA-PKcs was also incubated with the 54 bp DNA using a 1:6 protein:DNA molar ratio to ensure that a high proportion of DNA-PKcs molecules would contain DNA. Under these conditions, 1:1 protein:DNA complexes should be favoured. EM was performed and images from single molecules were separated into different sets congruent with unique volumes. Hence, all particles observed in the EM fields were selected and extracted without any *a priori* criteria, accounting for a total of 10 468 individual images. All of them were used in a 3D classification and refinement procedure independent of any previous volume (Ludtke *et al.*, 1999). An initial volume was generated after model-free image classifica-

tion and using common lines, which was then used to generate a set of projections with a uniform distribution of orientations. Each single image was classified using these projections as references. Two criteria were used to select particles congruent with a unique volume. First, within each class, only the more similar particles were used to generate an average. Secondly, this collection of new class averages was used to reconstruct a new volume, but only the classes that best matched this new structure were actually included in the reconstruction. During the first steps of the refinement process, volumes were built from a small percentage of the total number of initial particles but, after a few iterations, and keeping these two selection criteria, a congruent volume could be generated containing a few thousands images. The particles that were not included in this first volume were processed independently following similar procedures, and a new structure was obtained.

Therefore, we found that the initial set of particles could be classified into two sets of averages (Figure 3A and D), each one compatible with just one structure. A total of 3049 particles generated class averages (Figure 3A) congruent with one volume (Figure 3B and C) which correlated with the 3D structure obtained previously from images of DNA-PKcs without the addition of any ligand. On the other hand, 3280 particles not included in the first set (Figure 3D) built a volume different from any of the two previous structures (Figure 3E and F). The remaining particles could not be classified unambiguously into any of the volumes, and were discarded. The quality of the particle assignment to each volume was confirmed because, when the two resulting volumes were used as starting models for the other set of images (to force a bias in the refinement), the intermediate volumes during the processing evolved towards the previous structures. Consequently, we had resolved two complexes from our sets of images: DNA-PKcs (Figure 3A and C) and DNA-bound DNA-PKcs (Figure 3D and F). To reinforce this interpretation, DNA within the latter volume has also been identified (see below).

The DNA-PKcs structure at 30 Å resolution (Figure 3B and 3C) contains three distinct regions we have labelled as 'head', 'palm' and an 'arm' that connects the head to the palm. The head encloses a cavity surrounded by protein density and two openings in the front of the molecule. DNA-PKcs has a longitudinal axis of ~14 nm and a thickness ranging from 7 to 10 nm. This reconstruction closely resembles the previously published structure of the protein obtained by electron crystallography (Leuther *et al.*, 1999), though some clear differences are also visible and mainly located at the level of the 'palm' domain. In the crystal structure, this domain forms a compact block that contains a flexible arm, whereas in our 3D reconstruction this domain creates a palm-shaped feature. Upon inspection of the two volumes, these differences seem to be due to an ~90° rotation of the palm domain in our reconstruction compared with the crystallographic structure.

The 3D structure of ATM, at a similar resolution, has been solved recently (Llorca *et al.*, 2003; see inset in Figure 3B) using a single-particle EM approach, thus allowing direct comparison of the two structures. DNA-PKcs and ATM display strong structural similarities, including head and arm domains. Recently, it has been
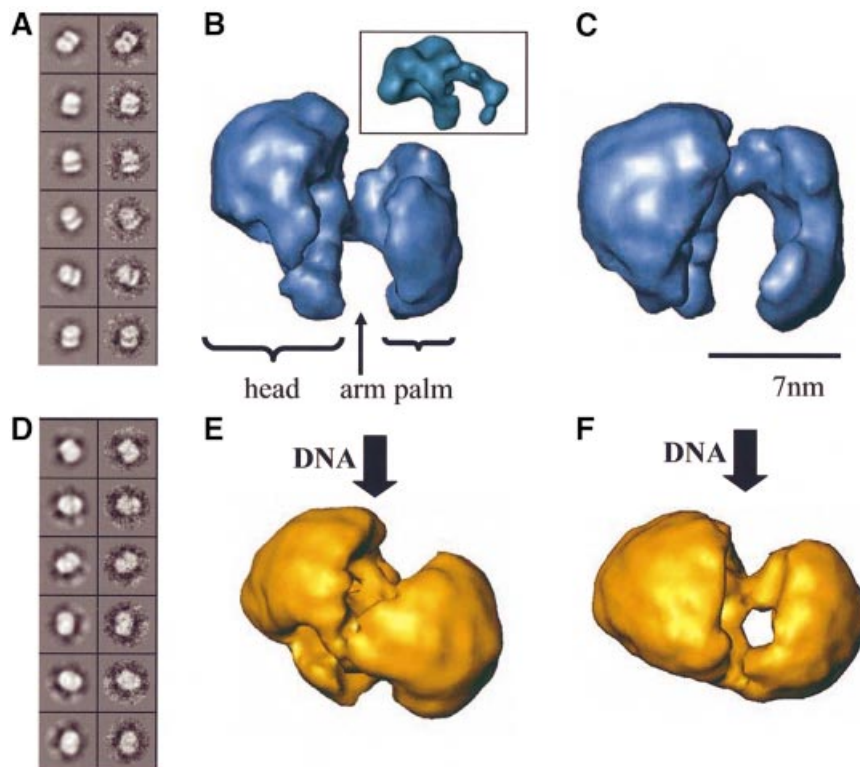
Fig. 3. 3D structure of DNA-PKcs and its DNA-bound complexes. (**A**) Classes from the DNA-PKcs volume. Each pair of images represents a projection from the final volume and the corresponding average from the original data. (**B** and **C**) Two views of the DNA-PKcs volume. The inset in (B) shows a comparable view of ATM. Scale bar represents 7 nm. (**D**) Classes from the DNA-bound structure. (**E** and **F**) Two views of the DNA-bound complex at similar orientations to those in (B and C).

reported that the PIKK family of kinases may share a common structural architecture based on a low sequence conservation helical unit known as HEAT repeats (Perry and Kleckner, 2003), and the 3D structures of DNA-PKcs and ATM support these hypotheses.

Conformational changes in DNA-PKcs upon DNA binding

DNA-bound DNA-PKcs, three-dimensionally reconstructed at 30 Å resolution, shows discernible head, arm and palm domains, but substantial conformational changes have taken place compared with the unbound protein (Figure 3E and F). Views of the DNA-free and DNA-bound complexes at compatible orientations are shown (Figure 3). The palm domain in the DNA-bound DNA-PKcs is bent and comes into contact with the head. In top views of the two reconstructions (Figure 3C versus F), these domain movements are most clearly visible. As a consequence of DNA binding, not only is the palm bending but also the arm moves inwards so that the palm actually achieves contact with the head (Figure 3F). As a result of all these modifications, a small channel is left between head and palm, which is sufficiently large to accommodate dsDNA. It is tempting to speculate that these DNA-driven conformational changes could be responsible for the activation of the kinase activity of DNA-PKcs that we observed in the presence of the 54 bp DNA.

Localization of the dsDNA in DNA-bound DNA-PKcs complexes

A common theme solving DNA–protein complexes by single-particle EM is the difficulty in the detection of the DNA component, perhaps due to DNA's flexibility or the way it interacts with the staining agent. The DNA-bound DNA-PKcs complex (Figure 3E and F) displays large conformational changes, but no DNA is clearly observed. However, when this volume is examined at a slightly lower threshold to visualize other structural features clearly still above the background noise, a long density comes out of the reconstruction (Figure 4A and B, white transparency superimposed to the same volume at the usual threshold). This density has the shape and dimensions that would be expected for a short segment of dsDNA. When the reconstruction from unbound DNA-PKcs, generated out of images from the same micrographs as the DNA-bound complex, was analysed using the same lower threshold, this extra density was never observed (unpublished data). This observation supports our view that we are in fact visualizing the DNA in the complex and, additionally, reinforces our claim that the original single images have been correctly assigned to either of the two volumes. The DNA comes out of the complex from just one side and in a reasonably well defined position. The lower threshold needed to observe the DNA density might reflect that we are averaging a small range of positions within the protein complex.
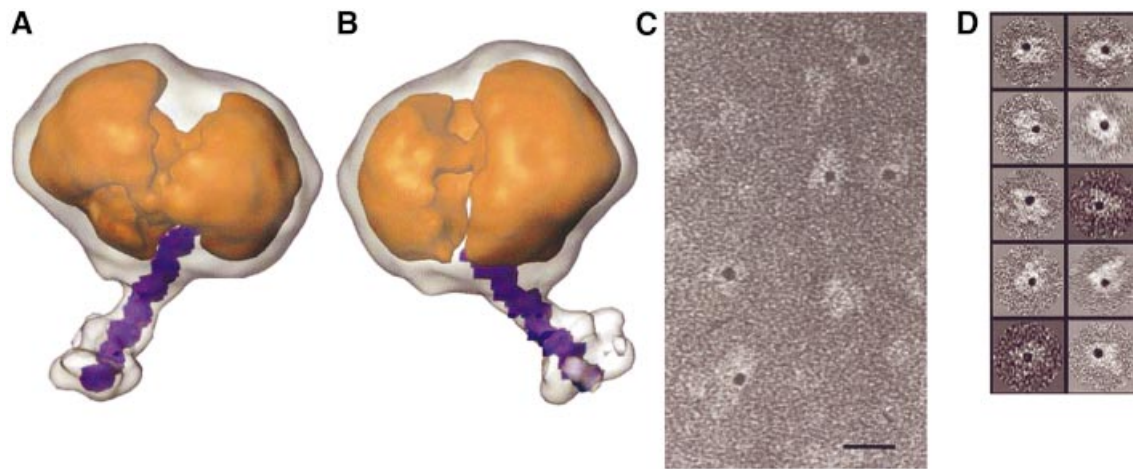
Fig. 4. Localization of DNA in the DNA-bound DNA-PKcs complexes. (**A** and **B**) Views of the DNA–DNA-PKcs volume at two different thresholds. The image at the lower threshold is shown as a white transparency superimposed on the volume at the usual threshold as an orange solid object. A 36 bp DNA was scaled to 4.9 Å/voxel, docked into the extra density and displayed in purple. (**C**) An area from micrographs where gold–DNA complexes were incubated with DNA-PKcs. (**D**) A gallery of selected individual images from (C).

As an independent method to detect the presence of DNA bound to DNA-PKcs in the images obtained by EM, we labelled the 54 bp oligo with a gold conjugate. A 5′-biotinylated derivative version of the DNA was incubated with a streptavidin-coupled gold conjugate with a gold particle of 5 nm in diameter to generate gold–DNA complexes. Gold–DNA was incubated with purified DNA-PKcs at a 1:1 molar ratio, and the preparation was added to grids and observed in the microscope. The presence of streptavidin–gold in one end of the DNA should preclude the interaction of DNA-PKcs, leaving just one free end at the opposite side. As controls for the specificity of the results, we also observed streptavidin–gold on its own, DNA-PKcs plus streptavidin–gold without DNA, and DNA-PKcs plus streptavidin–gold plus a non-biotinylated form of dsDNA (unpublished data). Only in the presence of the gold–DNA complex were a large number of DNA-PKcs molecules labelled with one gold particle observed (Figure 4C and D), and this confirms the presence of DNA-bound DNA-PKcs in our sample. Some gold densities were also found that were not associated with the protein, corresponding to free gold–DNA.

Model for kinase activation upon DNA binding

As shown in Figure 1, binding of the 54 bp DNA to DNA-PKcs strongly activated its kinase activity on its natural substrate, the XRCC4 protein. The DNA density coming out from DNA-bound DNA-PKcs could be docked very well to a 36 bp dsDNA (Figure 4A and B; DNA in purple within the white transparency). Therefore, it seems that ~18 bp, out of the 54 bp DNA, are in contact with DNA-PKcs. Previous studies indicate that a minimum length of ~15 bp of dsDNA was required to activate DNA-PKcs (Leuther *et al*., 1999; Hammarsten *et al*., 2000; Martensson and Hammarsten, 2002) and, although smaller dsDNA molecules bind with comparable affinity, they do not activate the kinase. Furthermore, increasing the length of the dsDNA beyond 20 bp does not elicit a further significant increase in kinase activation. When considered in light of our EM reconstruction, these data are most consistent with a model in which DNA-PKcs kinase activation on DNA binding may be the result of closure of the cavity between the head and palm. The stabilization of this conformational change could require a minimum of two points of contact between DNA-PKcs and dsDNA: (i) a binding site for the broken end of the DNA in the base of the palm; and (ii) an interaction between the edge of the head domain and the sugar–phosphate backbone of the DNA 15–20 bp out from the end, as the DNA emerges from the cavity between the head and palm (Figure 4A and B). An activating DNA molecule would thereby bridge the palm and head domains and stabilize the closed conformation, while a short dsDNA molecule would only occupy the end-binding site and would fail to activate the kinase. Extending the length of dsDNA over and above that required for making the bridging contact with the head would add no further stability to the closed conformation and would not further activate the kinase, consistent with the observed data.

Model for dsDNA recognition by DNA-PKcs and ATM

Previous reports have already provided information and some hypotheses on how DNA-PKcs could recognize DNA (Leuther *et al*., 1999; DeFazio *et al*., 2002). Some models suggest that both single-stranded and dsDNA are bound by DNA-PKcs through its different holes and cavities, and that a flexible subdomain could be used to mediate this interaction (Leuther *et al*., 1999; Martensson and Hammarsten, 2002). We show, for the first time, a comparison between the 3D structures of DNA-PKcs and a DNA-bound complex at medium resolution. We observe that upon DNA incubation, DNA-PKcs displays conformational changes that encircle the DNA through a clamp closure motion (Figure 5A and C). The gross mechanistic aspects of this model can be generalized to ATM (Figure 5D and F). The palm domain of DNA-PKcs can grab and encircle DNA, and this interaction takes place through DNA ends, which are somehow specifically recognized. During NHEJ, it is likely that the Ku protein
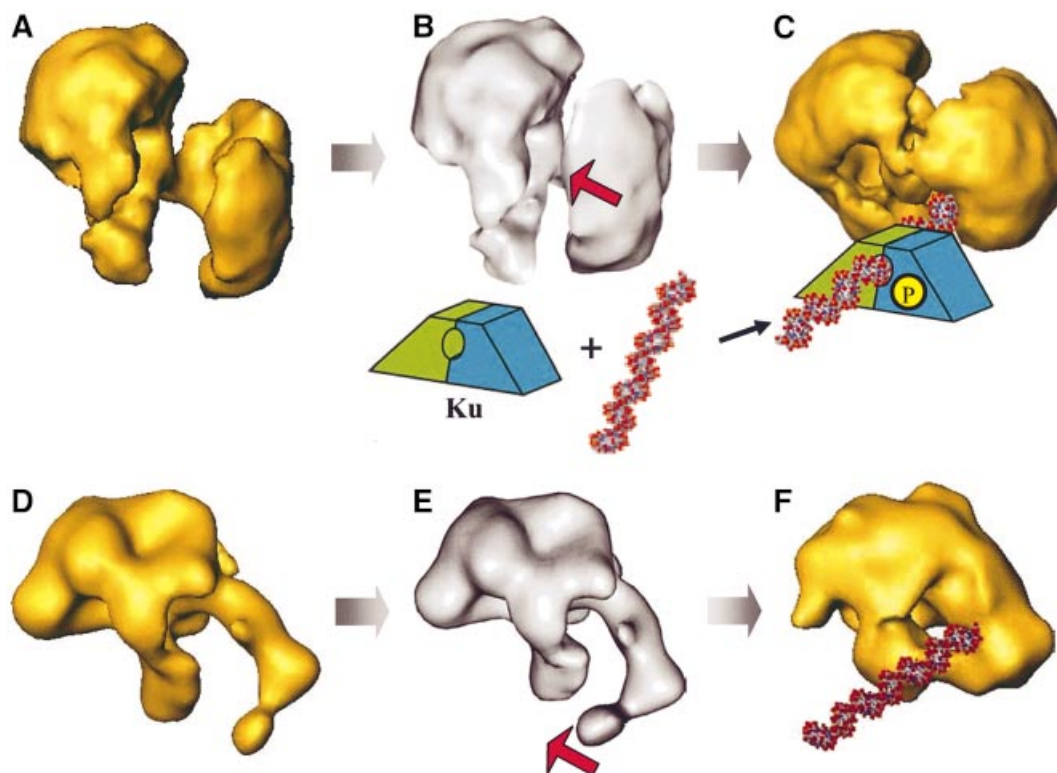
Fig. 5. Model for DNA recognition by DNA-PKcs (**A–C**) and ATM (**D–F**). (A and D) The apo-EM maps; (C) and (F) correspond to the DNA-bound reconstructions. (B and E) Theoretical intermediate states calculated using vibrational analysis and corresponding to the lowest-frequency normal mode captured from the DNA-PKcs (A) and ATM (D) DNA-free electron density maps. Red arrows indicate the direction of the conformational changes in the arm domains. P stands for inorganic phosphate.

acts as a recruiting factor to allow high affinity binding of DNA-PKcs to broken DNA. However, after Ku–DNA-PKcs interaction, Ku translocates into the DNA leaving DNA-PKcs at the DNA free end, bound probably through the conformational changes observed here. A Ku-like factor may also help ATM to bind to DNA, although it has not been included in the model. At this stage, DNA-PK could act as a scaffolding protein for the assembly of other components in the repair machinery. In addition, DNA-induced conformational changes probably activate the kinase to phosphorylate substrates implicated in DNA repair, including Ku itself. A minimum length of DNA is required to induce and stabilize these conformational changes and the subsequent kinase activation.

Prediction of domain motions using vibrational analysis

Vibrational analysis has been shown to be a powerful tool to predict potential motions of macromolecular machines where the low frequency modes efficiently describe the experimentally observed global domain movements (Ming *et al.*, 2002; Chacón *et al.*, 2003). We have carried out this type of analysis of both DNA-PKcs and ATM using their DNA-free EM density maps (Figure 5A and D) and without any other additional input information. The normal mode analysis was performed with an elastic model built from the EM structures with the help of vector quantization techniques to represent the density maps in real space with a number of landmark points. A total of 1000 landmarks with a connecting spring distance cut-off

of 14 Å were used. Normal mode analysis decomposed the possible motions of the elastic model in an orthonormal basis of modes (i.e. displacements) sorted by frequency. The first mode displacements were applied to the density maps by interpolation with the 3D thin-plate spline method (Bookstein, 1991). The amplitudes of the motions were scaled to better visualize the mode motion.

The intrinsic global flexibility of both proteins predicted large motions where the lowest frequency mode describes the closure of the palm domain towards the head domain in DNA-PKcs (Figure 5B and Supplementary movie1 available at *The EMBO Journal* Online) and the closure clamp motion of the arm-like domain in ATM (Figure 5E and Supplementary movie2). These predictions are in full agreement with the conformational changes we observed experimentally in our EM reconstructions (Figure 5C and F). These analyses support the likelihood of the conformational changes we have observed by EM and provide a model of how the transition between the DNA-free and DNA-bound conformations might take place. Note that even though the lowest frequency mode described the basic motions, other low frequency modes or a lineal combination of modes can complement the description of the movements (unpublished data).

In conclusion, we have found that both ATM (Llorca *et al.*, 2003) and DNA-PKcs are built with a similar general architecture where an equivalent structural region, the arm domain, is at the centre of the conformational changes upon DNA recognition. At least in the case of DNA-PKcs, these movements seem to be responsible for

the activation of its kinase activity, but we can hypothesize that other PIKK kinases might share these common properties during DNA binding.

Materials and methods

Sample preparation

DNA-PKcs was purified as previously described (Gell and Jackson, 1999) with a few modifications. Briefly, HeLa nuclear extract (Computer Cell Culture, Mons, Belgium) was fractionated on a Q-Sepharose column (Pharmacia) followed by a heparin–agarose column (Sigma). Fractions containing DNA-PKcs were separated by a phenyl-Sepharose column (Pharmacia) in 0.75 M ammonium sulfate, developed by a linear gradient of 0.75–0 M ammonium sulfate. DNA-PKcs-containing fractions were purified further by a Mono-S column (Pharmacia). Pure DNA-PKcs-containing fractions were pooled, dialysed against buffer A [25 mM HEPES pH 7.6, 50 mM KCl, 1 mM $MgCl_2$, 1 mM dithiothreitol (DTT), 0.5 mM EDTA and 20% glycerol] and stored at –80°C.

The 54 bp blunt-ended dsDNA was made by annealing two, HPLC- or PAGE-purified, complementary 54 base oligonucleotides (5′-GGCCG-CACGCGTCCACCATGGGGTACAACTACGATCTAGCTTCATGC-ACCGGAC-3′). The quality of the annealing was tested by measuring the hyperchromicity following digestion by snake venom phosphodiesterase 1 (Amersham).

Human XRCC4 was cloned from human kidney cDNA (Clontech) into pRSET-B (Invitrogen) and expressed in BL21-CodonPlus(DE3) cells (Stratagene). The His$_6$-tagged recombinant protein was purified by an immobilized metal-affinity column (Clontech) followed by ion exchange chromatography on a HiTrap-Q column (Pharmacia) and, finally, by gel filtration on a Superdex 200 column (Pharmacia). The purified XRCC4 was stored at –80°C in 20 mM Tris–HCl pH 8.0, 10% glycerol, 1 M NaCl, 1 mM EDTA, 2 mM DTT, 0.1 mM phenylmethylsulfonyl fluoride (PMSF).

Electrophoretic mobility shift assay (EMSA)

EMSA was carried out essentially as described (Hammarsten and Chu, 1998) with minor modifications. Binding reactions were performed in buffer B (10 mM Tris–HCl pH 7.5, 10 mM NaCl, 1 mM EDTA, 1 mM DTT and 5% glycerol) using 0.5 ng of ^{32}P-labelled dsDNA (54 bp). The protein was always added last, followed by 30 min incubation at room temperature. Protein–DNA complexes were resolved on a 4% polyacrylamide gel in $\times$0.25 TGE buffer at 4°C.

Kinase assays

The DNA-dependent kinase activity was tested by the phosphorylation of XRCC4 in the presence or absence of DNA. A 1 µg aliquot of XRCC4 was phosphorylated in the presence of 10 ng/µl DNA, 10 mM Tris–HCl pH 7.5, 50 mM KCl, 10 mM $MgCl_2$, 1 mM DTT, 2 µl of [γ-^{32}P]ATP (6000 Ci/mmol, 10 mCi/ml) and 200 ng DNA-PKcs, in a volume of 20 µl, for 30 min, at 30°C. The reaction products were analysed by SDS–PAGE, and the gel was stained with Coomasie blue, dried onto 3MM paper and developed by autoradiography. Protein bands corresponding to DNA-PKcs and XRCC4 were cut and the radioactivity was measured by Cerenkov counting.

Electron microscopy

A few microlitres of purified DNA-PKcs and its DNA-bound complexes were diluted to 0.2 mg/ml in buffer (50 mM Tris–HCl pH 7.5, 50 mM KCl, 1 mM $MgCl_2$ and 20% glycerol) and applied to carbon-coated grids. The sample was negatively stained with 2% uranyl acetate and observed in Philips CM100 and a JEOL 1230 electron microscopes. The microscopes were operated at 100 kV and the micrographs recorded at 0° tilt and a magnification of 39 000$\times$ under low dose conditions. A Leafscan45 scanner (Leaf Systems Inc.) was used to scan the pictures with a 10 µm step size.

Image processing and three-dimensional reconstructions

A total of 2746 particles from purified DNA-PKcs and 10 468 particles from the DNA incubated sample were selected from the micrographs at a final 4.9 Å/pixel using XMIPP (Marabini et al., 1996). Particles initially were centred and averaged in two dimensions using XMIPP. Image classification and 3D refinement were carried out without assuming any starting model using EMAN (Ludtke et al., 1999). Resolution was estimated by Fourier shell correlation between two independent volumes. Using the criteria of a 0.5 correlation coefficient, the volumes showed a

resolution of 30 Å. The handedness of the structure was determined by comparison with the absolute handedness calculated from 2D crystals (Leuther et al., 1999). Docking of the 36 bp DNA into the DNA-bound volume was done after scaling to 4.9 Å/voxel.

Gold labelling

Streptavidin–gold with a gold particle of 5 nm in diameter (BB International) was incubated with a 5′-biotinylated 54 bp DNA to generate gold–DNA complexes. Afterwards, DNA-PKcs was incubated with the pre-formed gold–DNA complex for 15 min at a 1:1 molar ratio, which is lower than that used in the 3D reconstructions, in order to avoid a strong background of free gold–DNA in the EM fields. The reaction was applied to carbon-coated grids, negatively stained and observed in the electron microscope.

Vibrational analysis

The full procedure to carry out this analysis has already been described in detail (Chacón et al., 2003). Briefly, a normal mode analysis is performed with an elastic model built from a given EM structure, DNA-free ATM (Llorca et al., 2003) and DNA-PKcs in our case. Normal mode analysis decomposes the possible motions of the elastic model in an orthonormal basis of modes (i.e. displacements) sorted by frequency. The low frequency modes have been found to capture efficiently the functional global motions exhibited by large macromolecules (Chacón et al., 2003).

Supplementary data

Supplementary data are available at *The EMBO Journal* Online.

Acknowledgements

References

Bakkenist,C.J. and Kastan,M.B. (2003) DNA damage activates ATM through intermolecular autophosphorylation and dimer dissociation. *Nature*, **30**, **421**, 499–506.

Bookstein,F.L. (1991) *Morphometric Tools for Landmark Data*. Cambridge University Press, Cambridge.

Chacón,P., Tama,F. and Wriggers,W. (2003) Mega-Dalton biomolecular motion captured from electron microscopy reconstructions. *J. Mol. Biol.*, **326**, 485–492.

Chan,D.W. and Lees-Miller,S.P. (1996) The DNA-dependent protein kinase is inactivated by autophosphorylation of the catalytic subunit. *J. Biol. Chem.*, **271**, 8936–8941.

Chiu,C.Y., Cary,R.B., Chen,D.J., Peterson,S.R. and Stewart,P.L. (1998) Cryo-EM imaging of the catalytic subunit of the DNA-dependent protein kinase. *J. Mol. Biol.* **284**, 1075–1081.

Critchlow,S.E., Bowater,R.P. and Jackson,S.P. (1997) Mammalian DNA double-strand break repair protein XRCC4 interacts with DNA ligase IV. *Curr. Biol.*, **7**, 588–598.

DeFazio,L.G., Stansel,R.M., Griffith,J.D. and Gilbert,C. (2002) Synapsis of DNA ends by DNA-dependent protein kinase. *EMBO J.*, **12**, 3192–3200.

Gell,D. and Jackson,S.P. (1999) Mapping of protein–protein interactions within the DNA-dependent protein kinase complex. *Nucleic Acids Res.*, **27**, 3494–3502.

Hammarsten,O. and Chu,G. (1998) DNA-dependent protein kinase: DNA binding and activation in the absence of Ku. *Proc. Natl Acad. Sci. USA*, **95**, 525–530.

Hammarsten,O., DeFazio,L.G. and Chu,G. (2000) Activation of DNA-dependent protein kinase by single-stranded DNA ends. *J. Biol. Chem.*, **275**, 1541–1550.

Jackson,S.P. (2002) Sensing and repairing DNA double-strand breaks. *Carcinogenesis*, **23**, 687–696.

Leuther,K.K., Hammarsten,O., Kornberg,R.D. and Gilbert,C. (1999) Structure of DNA-dependent protein kinase: implications for its regulation by DNA. *EMBO J.*, **18**, 1114–1123.

Llorca,O. *et al.* (2001) The 'sequential allosteric ring' mechanism in the eukaryotic chaperonin-assisted folding of actin and tubulin. *EMBO J.*, **20**, 4065–75.

Llorca,O., Rivera-Calzada,A., Grantham,J. and Willison,K.R. (2003) Electron microscopy and 3D reconstructions reveal that human ATM kinase uses an arm-like domain to clamp around double-stranded DNA. *Oncogene*, **22**, 3867–3874.

Ludtke,S.J., Baldwin,P.R. and Chiu,W. (1999) EMAN: semi automated software for high-resolution single-particle reconstructions. *J. Struct. Biol.*, **128**, 82–97.

Marabini,R. *et al.* (1996) Xmipp: an image processing package for electron microscopy. *J. Struct. Biol.*, **116**, 237–240.

Martensson,S. and Hammarsten,O. (2002) DNA-dependent protein kinase catalytic subunit. *J. Biol. Chem.*, **277**, 3020–3029.

Merkle,D. *et al.* (2002) The DNA-dependent protein kinase interacts with DNA to form a protein–DNA complex that is disrupted by phosphorylation. *Biochemistry*, **41**, 12706–12714.

Ming,D., Kong,Y., Wakil,S.J., Brink,J. and Ma,J. (2002) Domain movements in human fatty acid synthase by quantized elastic deformational model. *Proc. Natl Acad. Sci. USA*, **99**, 7895–9.

Perry,J. and Kleckner,N. (2003) The ATRs, ATMs and TORs are giant HEAT repeat proteins. *Cell*, **112**, 151–155.

Pierce,A.J. and Jasin,M. (2001) NHEJ deficiency and disease. *Mol. Cell*, **8**, 1160–1161.

Rouse,J. and Jackson,S.P. (2002) Interfaces between the detection, signalling and repair of DNA damage. *Science*, **297**, 547–551.

Shiloh,Y. (2003) ATM and related protein kinases: safeguarding genome integrity. *Nature Rev. Cancer*, **3**, 155–168.

Soubeyrand,S., Pope,L., Pakuts, B and Hache,R.J. (2003) Threonines 2638/2647 in DNA-PK are essential for cellular resistance to ionizing radiation. *Cancer Res.*, **15**, 1198–1201.

West,R.B., Yaneva,M. and Lieber,M.R. (1998) Productive and non-productive complexes of Ku and DNA-dependent protein kinase at DNA termini. *Mol. Cell. Biol.*, **18**, 5908–5920.

Yaneva,M., Kowalewski,T. and Lieber,M.R. (1997) Interaction of DNA-dependent protein kinase with DNA and with Ku: biochemical and atomic-force microscopy studies. *EMBO J.*, **16**, 5098–5112.